

1 **Strategies to improve light utilisation in solar fuels synthesis**

2 Qian WANG,^{1,2,3†} Chanon PORNRUNGROJ,^{1,†} Stuart LINLEY,¹ Erwin REISNER^{1,*}

3

4 **Affiliation and full postal address**

5 1 *Yusuf Hamied Department of Chemistry, University of Cambridge, Lensfield Road, Cambridge*

6 *CB2 1EW, UK*

7 2 *Graduate School of Engineering, Nagoya University, Furo-cho, Chikusa-ku, Nagoya 464-8603,*

8 *Japan*

9 3 *Institute for Advanced Research, Nagoya University, Furo-cho, Chikusa-ku, Nagoya 464-8601,*

10 *Japan*

11 † Equal contribution

12 *Corresponding author

13 Professor Erwin REISNER

14 *Yusuf Hamied Department of Chemistry, University of Cambridge, Lensfield Road, Cambridge CB2*

15 *1EW, UK*

16 Tel: +44-1223336323

17 E-mail: reisner@ch.cam.ac.uk

18 Website: www-reisner.ch.cam.ac.uk/

19

20 **Abstract**

21 The synthesis of fuels using sunlight offers a promising sustainable solution for chemical energy
22 storage, but inefficient utilisation of the solar spectrum limits its commercial viability. Apart from
23 fundamental improvements to (photo)catalyst materials, solar fuel production systems can also be
24 designed to improve solar energy utilisation by integrating complementary technologies that more
25 efficiently utilise the solar spectrum. Here we review recent progress on emerging complementary
26 approaches to better modify, enhance, or distribute solar energy for sunlight-to-fuel conversion,
27 including advanced light management, integrated thermal approaches, and solar concentrators. These
28 strategies can improve the efficiency and production rate of existing photo(electro)chemical systems
29 and, therefore, the overall economics of solar fuel production. More broadly, the approaches highlight
30 the necessary collaboration between materials science and engineering to help drive the adoption of
31 a sustainable energy economy in the near future using existing technologies.

32

33 Solar-driven photo(electro)chemical systems utilise solar energy to split water (H_2O) and
34 convert carbon dioxide (CO_2) to produce hydrogen gas (H_2) and carbon-based fuels in a process
35 usually referred to as ‘artificial photosynthesis’. Many artificial photosynthetic technologies exist in
36 various stages of development, and these can be broken down into the following three main
37 categories: photocatalysis, photoelectrochemistry, and photovoltaic-driven electrolysis (PV-
38 electrolysis) (**Figure 1a-c**).¹ However, techno-economic analyses have shown that none of current
39 laboratory-scale technologies meet the criteria for practical sustainable fuel production due to
40 insufficient solar-to-chemical conversion efficiency (η_{chem}), the absence of catalysts that are highly
41 active and selective, and unsatisfactory scalability and stability.²

42 In general, PV-electrochemical systems benefit from commercially available components and
43 already display high η_{chem} . Nonetheless, PV-electrochemical and photoelectrochemical devices still
44 face technical challenges due to high materials and manufacturing costs, mass transport limitations,
45 and substantial resistive losses that must be addressed before such systems can be efficiently scaled
46 up.³ In contrast, photocatalytic systems are relatively simple, requiring far less auxiliary hardware,
47 and are therefore expected to generate solar fuels more cost-effectively on a large scale, even though
48 the η_{chem} of such systems are currently limited to 1-2%.^{4,5} Economic viability of solar fuels from
49 artificial photosynthesis may be achieved by reducing the fabrication and operation costs, improving
50 η_{chem} without substantial increases to costs, or employing low-cost materials and auxiliary systems
51 at sufficient scale (or with high enough production rates) to meet fuel production cost-thresholds
52 despite relatively low efficiency.

53 This review presents a range of complementary solar technologies, including light management,
54 photon wavelength manipulation, solar concentration, and thermal-related approaches to maximise
55 solar energy utilisation for the synthesis of chemical fuels. We discuss the benefits of such approaches
56 in terms of increasing η_{chem} and production rates, which can further enhance the best existing solar

57 fuel technologies to achieve economic viability. Implementing these complementary approaches will
58 require collaboration of a multidisciplinary research community and accelerate the realisation of
59 practical devices.

60

61 **Light management**

62 According to thermodynamic analysis based on a thermo-chemical equilibrium between the Sun
63 and a semiconductor, η_{chem} reaches an entropy-limited ideal maximum of 67% under 1 sun
64 irradiation (100 mW cm^{-2}), assuming all the photogenerated electron-hole pairs without
65 recombination can be used to produce storable chemical energy in artificial photosynthesis (**Table**
66 **1**).⁶ However, thermalisation of super-bandgap photons ($E > E_g$; E_g : bandgap) and the inability to
67 absorb sub-bandgap photons ($E < E_g$) amount to considerable combined losses.⁷ Owing to the
68 mismatch between photon energy and a given semiconductor bandgap across the entire solar spectrum,
69 a maximum achievable efficiency exists and is known as the Shockley–Queisser limit.⁸ Thus, the
70 theoretical maximum η_{chem} of a photo(electro)chemical system based on single light absorber
71 decreases to ~30% (under 1 sun irradiation) when considering thermalisation losses in addition to
72 entropy increase (**Table 1**).

73 **Figure 2** shows representative experimental systems with their solar-to-hydrogen conversion
74 efficiency (η_{H_2}), all of which are much lower than the theoretical maximum values based on the
75 thermo-chemical equilibrium analysis. One of the most significant challenges in realising efficient
76 solar fuel production is utilisation of the full solar spectrum. The infrared (IR) region, which accounts
77 for approximately 50% of total solar irradiance, cannot usually contribute directly to artificial
78 photosynthesis because its photon energies are smaller than the semiconductors' bandgaps and
79 contain less energy than needed for typical processes (e.g. water splitting; 1.23 eV at 1 atm and 25 °C).
80 Accordingly, reports of visible-light-driven artificial photosynthesis using single light absorber

81 photocatalytic without sacrificial reagents remain scarce due to stringent thermodynamic and kinetic
82 requirements.⁹

83 Instead, Z-scheme (tandem) systems using two light-absorbers that combine smaller bandgap
84 semiconductors are constructed and provide a higher maximal efficiency due to less restrictive or
85 complementary light absorption.¹⁰ For example, the front/top photoelectrode in a
86 photoelectrochemical tandem cell is transparent with a wider bandgap (E_{g1}) to absorb short-
87 wavelength light, allowing the penetration of long-wavelength light for utilisation by the back/bottom
88 photoelectrode which has a narrower bandgap (E_{g2}) (**Figure 1b**), thereby avoiding competition
89 between the two light absorbers and minimising thermalisation.^{11,12} Tandem cells with good light
90 management represent an effective way to reduce thermalisation losses, and a theoretical tandem cell
91 consisting of infinitely many light absorbers with different bandgaps estimates a maximum η_{chem} of
92 86% or 67% for 45900 suns and 1 sun intensities, respectively.^{6,11}

93 A key challenge is the search for a low-cost transparent front/top photoelectrode with both high
94 transmittance of longer wavelengths and sufficient absorbance of shorter wavelengths. BiVO_4 (E_g :
95 2.4 eV) shows high transmittance of wavelengths >500 nm and it has been widely used as a relatively
96 inexpensive and stable photoanode in bias-free photoelectrochemical tandem cells.^{13,14} A recent
97 efficiency milestone demonstrated an η_{H_2} of 19% for unbiased water splitting using $\text{Ga}_{0.41}\text{In}_{0.59}\text{P}$ (E_{g1}
98 = 1.78 eV) as the top photocathode coupled to a $\text{Ga}_{0.89}\text{In}_{0.11}\text{As}$ ($E_{g2} = 1.26$ eV) bottom photoanode
99 under 1 sun irradiation.¹⁵ In a tandem configuration, the optimal E_{g1} and E_{g2} have been estimated as
100 1.9 and 1.0 eV, respectively, attaining an ideal maximum η_{chem} of $\sim 42\%$ under 1 sun.¹¹ Accounting
101 for realistic losses in a photo(electro)chemical system, including electrode polarisation, overpotential
102 requirement for catalysis (0.6–0.8 eV), and solution resistance, results in an optimal E_{g1} and E_{g2} of
103 ~ 1.6 and ~ 1.0 eV, respectively, with a maximum η_{H_2} of $\sim 27\%$.^{12,16}

104 Spectral beam splitting is used extensively to address the spectral mismatch problem of photonic
105 devices. Sunlight can be split into several bands using strategies such as dichroic mirrors, holographic
106 concentrators, and rugate filters.¹⁷ Spectral beam splitting in an integrated PV-driven
107 photoelectrochemical system, where PV cells provide an extra bias for the photoelectrochemical
108 device, allows wavelength bands to be directed to the most efficient converter. For example, directing
109 ultraviolet (UV) and short visible wavelengths to a photoelectrochemical device while the long visible
110 wavelengths and near-infrared (NIR) are directed to a solar cell maximises solar energy utilisation
111 (**Figure 3a**).¹⁸ As an example, a beam splitter was integrated into a PV-photoelectrochemical system
112 consisting of a photoelectrochemical element with a Mo-doped BiVO₄ (BiVO₄:Mo) photoanode
113 modified with a water-oxidising Fe(Ni)OOH catalyst and a H₂-evolving Pt cathode connected to a
114 single-junction perovskite PV cell, producing a η_{H_2} of ~6% for water splitting.¹⁹ The beam splitter
115 separated solar irradiation (1 sun) into two light beams, directing wavelengths >515 nm to the solar
116 cell and wavelengths <515 nm to the BiVO₄:Mo photoanode.

117 Another feature of the beam splitter is the possibility of filtering the spectrum to avoid heating
118 of PV devices, which can increase the durability and efficiency of solar cells,^{17,20} instead redirecting
119 the heat to enhance catalysis processes. However, beam splitters always introduce energy losses (~1–
120 3%),²¹ which must be offset by the resulting decrease in thermalisation losses. Careful design of such
121 devices is necessary as the elastic energy stored in thick, multi-layer coatings can cause internal
122 stresses which reduce the durability and lead to cracking or delamination.²¹ Ultimately, the increased
123 cost of fabricating quality splitters with tight optical tolerances and high durability must be justified
124 by the gain in efficiency.

125 One, two, or three-dimensional periodic dielectric structures or gratings,²² and isotropically
126 scattering (or Lambertian) surfaces²³ are commonly used in the PV community to increase the
127 absorption and solar-to-electricity conversion efficiency (η_{elec}) of solar cells via light trapping. Light

128 trapping schemes are generally based on geometric structures or features that elongate the optical
129 path length through random scattering from a roughened front surface and reflective back surface.²⁴
130 Solar cell transmission losses can be reduced by guiding light multiple times into its absorbing region,
131 increasing the optical path length of the light, and thereby the probability of light absorption, while
132 keeping its physical thickness unaltered.²⁴

133 Based on these advantages, light-trapping is also a promising strategy for improving efficiency
134 of photoelectrochemical and photocatalytic systems, as shown in **Figure 3b**. In particular, the front
135 photoelectrode in tandem devices is expected to effectively harvest super-bandgap photons while
136 being transparent enough to feed the back absorber with sub-bandgap photons. As an example of a
137 light-trapping strategy, a distributed Bragg reflector designed to reflect <500 nm and transmit >500
138 nm light was installed between a BiVO₄/WO₃ photoanode and a dye sensitised solar cell to increase
139 the light utilisation of the PV-photoelectrochemical tandem device resulting in a 24% improvement
140 to photocurrent and a η_{H_2} of 7.1%.²⁵ Through such a photon recycling strategy, the trade-off between
141 light absorption and transmittance for the front photoelectrode can be lessened. Additionally,
142 fabricating thin-film photoelectrode and solar cell assemblies with an active layer thickness in the
143 range of hundreds of nanometers has the advantage of reduced material usage, shorter carrier
144 collection lengths, and lower series resistance.²⁴

145

146 **Solar spectrum adaptation**

147 Efficiencies exceeding the Shockley–Queisser limit can be reached by converting the solar
148 spectrum to wavelengths that match the absorption edge of the light absorber; an approach that has
149 received the most attention in solar cells and is comparatively underdeveloped in solar fuel production
150 devices. By doing so, energy from sub-bandgap photons and excess energy from super-bandgap
151 photons can contribute to the quantum efficiency (QE; the ratio of charge carriers used for current

152 generation/chemical reaction to incident photons) of the device, sidestepping the Shockley–Queisser
153 assumption that this energy would otherwise be lost.

154 The thermalisation of charge carriers caused by the absorption of super-bandgap photons is one
155 of the major loss mechanisms leading to low efficiency, particularly in the case of narrow-bandgap
156 semiconductors. Downconversion (quantum cutting) (**Figure 4a**) splits one high-energy photon into
157 two lower-energy photons that can each excite an electron-hole pair.⁷ For example, singlet exciton
158 fission is a downconversion process in organic semiconductors, spontaneously converting one spin-
159 singlet electron-hole pair into two spin-triplet excitons.^{26,27} This process can reduce energy loss
160 related to the thermalisation of hot charge carriers, predicting an upper η_{elec} limit of ~40% for PV
161 systems (single light absorber, E_g : ~1.0 eV) under 1 sun.^{28,29} By cutting one high-energy photon into
162 two low-energy photons that can both be absorbed by the semiconductor, the current generated from
163 photons with $E \geq 2E_g$ can be doubled.

164 Another process, down-shifting (**Figure 4b**), transforms one absorbed high-energy photon into
165 one lower-energy photon with a wavelength change known as the Stokes shift.⁷ Down-shifting is
166 useful for improving the η_{elec} of PV by shifting short-wavelength sunlight to the longer-wavelength
167 region where the semiconductor exhibits higher QE due to less surface recombination.³⁰ Lanthanide
168 ions, quantum dots, singlet fission materials and organolanthanide complexes have been explored as
169 wavelength-shifting materials.^{7,27}

170 Sub-bandgap photons are transmitted through semiconductors, resulting in limited utilisation of
171 photons. Upconversion is a process that absorbs low energy photons and ‘combines’ their energies,
172 re-emitting a photon with $E \geq E_g$. This technique offers a means of mitigating transmission losses and
173 increasing the η_{elec} of PV (single light absorber, E_g : 1.76 eV) to a limit of ~43% under 1 sun.²⁸ This
174 anti-Stokes emission can be achieved through two main pathways: lanthanide-doped upconversion
175 nanoparticles and triplet-triplet annihilation systems.³¹ The lanthanide ions possess multiple long-

176 lived and ladder-like electronic states, allowing even two- to six-photon upconversion processes to
177 realise large anti-Stokes shifts from NIR excitation to visible and UV emission. In triplet–triplet
178 annihilation-based upconversion, the photon energy absorbed by a sensitiser is transferred to an
179 acceptor, and two excited acceptors undergo triplet–triplet annihilation, producing upconverted
180 singlet fluorescence.

181 The η_{chem} of standalone photoelectrochemical tandem cells is very sensitive to the shape and
182 current densities at the intersection point of current density–voltage (J-V) curves of the two individual
183 photoelectrodes.¹² The J-V curve of a photoelectrode can be readily tuned by manipulating the
184 sunlight and enhancing the intensity of absorbable portion, leading to an increased operating current
185 density (J_{op}) and η_{chem} , as shown in **Figure 4c**. Estimates have demonstrated that the limiting η_{elec}
186 (and η_{chem} assuming that electrical energy can be transformed into chemical energy without loss) of
187 these semiconductors under 1 sun irradiation can be improved by a factor of ~1.8–2.8 when
188 combining ideal photon up- and down-conversion, reaching 45% when the bandgap is 0.9–1.4 eV
189 (**Table 1**).²⁸

190 Moreover, product selectivity of a standalone photoelectrochemical tandem cell for water
191 splitting and CO₂ conversion is sensitive to the shared electrode potential (operating potential V_{op}),³²
192 where photoelectrodes generate both photocathodic and photoanodic currents. By using solar
193 spectrum adaptation to adjust the V_{op} , control over the selectivity of desired products may be possible
194 (**Figure 4c**).

195 As an example of combined up- and down-conversion, a luminescent back reflector (LBR)
196 consisting of an organic fluorophore pair *meso*-tetraphenyltetrabenzoporphine palladium (PdTPBP)
197 and perylene, has been applied to increase the fraction of light usable by a BiVO₄:Mo photoelectrode
198 connected to a Pt cathode for overall water-splitting with external bias.³³ BiVO₄:Mo absorbs light
199 most efficiently at a wavelength of ~470 nm, therefore the LBR was designed to absorb light in the

200 wavelength ranges of 350–450 nm and 600–650 nm, and emit light at 470 nm. Specifically, the
201 PdTPBP absorbed 600–650 nm light and re-emitted it at 470 nm by Dexter energy transfer and triplet-
202 triplet annihilation, whereas perylene facilitated conversion from 350–450 nm to 470 nm through
203 down-shifting. The LBR enhanced the photocurrent density over an applied potential range of 0.3–
204 1.23 V (versus reversible hydrogen electrode (RHE)), experimentally demonstrating a modest
205 increase from 4.48 to 5.25 mA cm⁻² at 1.23 V_{RHE}.

206 Wide-bandgap photocatalysts that are only active under UV light would greatly profit from
207 highly efficient hybrid upconversion systems. Despite their large bandgaps, most research still
208 focuses on oxide materials because they are cheap, stable, and easy to prepare.^{4,9} By incorporating
209 upconversion materials to absorb lower-energy photons and emit higher-energy photons in the
210 absorbable range of a wide-bandgap photocatalyst ($E_g > 3.0$ eV) as shown in **Figure 4d and e**, the
211 limiting η_{elec} (and η_{chem} assuming that no loss in electrical-to-chemical energy conversion) under 1
212 sun irradiation may be improved from ~2 to 40%.³⁴ An example is given by a hybrid electrode
213 composed of hematite (α -Fe₂O₃, $E_g = 2.1$ eV) films and upconversion rare-earth nanocrystals
214 (NaYF₄:Yb,Er),³⁵ in which the nanocrystals absorb IR radiation (980 nm) and emit at 550 and 670
215 nm. Hence, photon energy from incident light in the IR range was rendered usable by hematite that
216 absorbs only UV and a part of visible radiation, resulting in water splitting driven by a 980 nm laser
217 with a QE = 1.24×10^{-4} % at 1.43 V_{RHE}.

218 The main drawback of using lanthanide-doped upconverters is their low upconversion efficiency
219 — generally well below 5% due to their narrow light absorption range.^{31,36} Triplet-triplet annihilation
220 systems suffer from a relatively small anti-Stokes shift and low stability, requiring specific operating
221 conditions (e.g. anoxic, non-aqueous) for efficient conversion.^{31,37} The oxygen sensitivity can be
222 diminished if the converter's triplet-state energies are below oxygen's singlet-state energy ($^1\Delta_g$ O₂ =
223 0.98 eV), and under certain conditions, the presence of oxygen can enhance upconversion.³⁸

224 Alternatively, additional engineering (*e.g.* enclosed in microcapsules) may facilitate operation in
225 ambient, oxygen-rich aqueous phase environments.³⁹ To increase the efficiency of photon
226 upconversion, hybrid upconversion nanosystems combining organic dyes and inorganic nanoparticles,
227 especially in the form of dye-sensitised lanthanide-doped upconversion nanoparticles, nanoparticle-
228 sensitised molecular triplet-triplet annihilation systems, and metal–organic-framework nanoparticles,
229 have been developed and offer exciting opportunities for applications with photonic devices.³¹ Down-
230 conversion has been reported with quantum efficiencies above 100%,⁴⁰ and exhibits the potential to
231 improve η_{elec} of PV with a single light absorber to ~40% (**Table 1**), yet challenges remain in the
232 integration into the devices and the stability in ambient conditions.

233

234 **Solar concentrators**

235 PV-electrochemical and photoelectrochemical systems suffer from scale-up issues due to their
236 complex fabrication processes and area-related costs including the price of reactors, module and
237 encapsulation, installation, and cabling. Concentrating solar power offers a way to improve the
238 production rate and efficiency of these systems, achieving concentrated fuel production on a smaller
239 active material footprint, thereby reducing the overall system cost. Practical solar concentrators focus
240 light onto devices with small areas following the basic optical principles of Snell’s law for reflection
241 by specular surfaces using parabolic mirrors, Fresnel lenses, dish–collectors, or heliostat power
242 towers.⁴¹

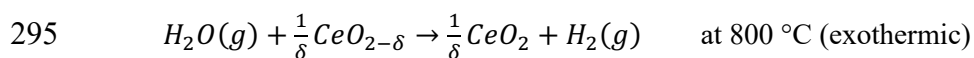
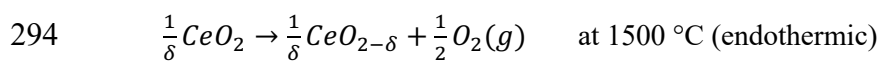
243 In PV systems, the use of concentrated sunlight benefits η_{elec} due to the increase of both current
244 (linearly) and voltage (approximately logarithmically) up to a saturation point, where resistance losses
245 prevent further increases in efficiency.^{42,43} The same is not true for η_{chem} in photo(electro)chemical
246 devices where efficiency is only dependent on the linear increase in current provided by concentrated
247 irradiation. High-efficiency concentrated photovoltaic (CPV) devices operating under concentrated

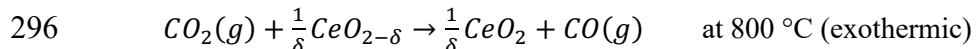
248 sunlight have been directly coupled with electrolysis cells: for example, a PV-electrochemical water
249 splitting system with an η_{elec} of 39% reported a record η_{H_2} of >30% using two electrolyzers under
250 42 suns irradiation.⁴⁴ Recent efforts have demonstrated a six-junction III-V solar cell with η_{elec} of
251 47.1% under 143x solar concentration.⁴⁵ Coupled with optimised electrolyser systems, such CPV
252 devices have the potential to further increase η_{H_2} above the current record of 31.2%. Even so, working
253 at such elevated current densities for PV introduces complexities such as excessive operating
254 temperatures and overpotentials, which can exacerbate degradation of the light-absorbing materials.⁴⁶
255 Since the required operating temperature of PV is lower than that of electrolysis, controlled heat
256 exchange between the two components is a promising way to improve device lifetime.⁴⁷ As a
257 consequence, a thermally integrated PV-electrochemical H₂-generation device, where controlled flow
258 of electrolyte was used to facilitate heat exchange, was stable for over 100 h in a water decomposition
259 system and achieved η_{H_2} of ~18% under 207 suns irradiation, while maintaining a working
260 temperature below 30 °C.⁴⁸

261 In addition to η_{chem} , production rate is another key metric in solar fuel production. A recent
262 techno-economic analysis on photocatalytic reforming of waste organics to H₂ suggested that a four-
263 fold increase in H₂ production rate would lower the cost of hydrogen production by 76% and
264 quadruple the energy returned on energy invested.⁴⁹ In a pair of experimental demonstrations, the
265 apparent rate constant (k_{app}) for photocatalytic production of H₂ over Au/TiO₂ was found to be
266 proportional to light intensity (I) through the relationship $k_{app} = k \cdot I^{0.65}$ at 25 °C and increase with
267 temperature according to an Arrhenius relationship, seeing a six-fold increase in rate over a
268 temperature increase of 50 °C at 1.5 mW cm⁻² UV-A irradiance (320–400 nm).^{50,51} Increased light
269 intensity and temperature for photocatalytic solar fuels processes, achieved through use of solar
270 concentrators, shows the possibility of achieving economic feasibility at higher production rates
271 through reactor design.^{50,52}

272 Some drawbacks of adopting solar concentrators are that only direct sunlight can be concentrated
 273 on the receiver effectively (thus losing energy from diffuse sunlight), and that both optical and
 274 resistive losses are more significant under concentration.⁴³ To obtain the optimal concentration at the
 275 receiver for solar fuel production, the daily and seasonal motion of the Sun must be considered. Hence,
 276 tracking-integrated concentrating systems, where the module is physically adjusted to optimise the
 277 collector's acceptance angle, are anticipated to be employed for solar fuel production systems (**Figure**
 278 **5a**). The integration of a tracking system allows the elimination of cosine losses which affect fixed-
 279 angle systems and may offset the efficiency loss incurred by failing to capture diffuse sunlight with
 280 a solar concentrator. The fraction of diffuse sunlight in Air Mass 1.5 Global spectrum (AM1.5G) is
 281 10%, but on cloudy or hazy days, or at higher air mass, this fraction can increase substantially and
 282 proportionally diminish the efficacy of the solar collector.⁴³ Overall, tracking-integrated solar
 283 concentration is believed to reduce system and maintenance costs, and their compact geometry would
 284 allow them to be opened up to the growing residential market.⁵³

285 Apart from the increased light intensity, solar concentrators also focus thermal energy which can
 286 be readily harvested. Using a variety of mirror designs, sunlight can be focused onto a relatively small
 287 absorber area, generating high temperatures typically ranging from 200 °C to 1500 °C.⁵⁴ This
 288 concentrated solar energy (5000 suns and beyond) has been proposed as useful for increasing or
 289 controlling heat to perform other solar fuel generation processes, such as solar thermolysis, solar
 290 thermochemical cycles, solar reforming, solar cracking, and solar gasification (**Figure 1d**).⁵⁵ For
 291 example, η_{chem} of 0.8% and 0.7% for CO₂ and H₂O splitting to produce CO and H₂, respectively,
 292 were achieved using porous monolithic CeO₂ in a state-of-the-art solar-cavity receiver reactor
 293 following the two-step thermochemical reactions:⁵⁴





297 This system demonstrated stable fuel generation over 500 cycles. Such two-step thermochemical
298 reactions based on metal oxide redox cycles are capable of producing H₂ at more technically feasible
299 reduction temperatures (1200 to 1500 °C) compared to direct thermolysis (>2700 °C).⁵⁶ Additionally,
300 since only the first step is endothermic, the second step can be carried out at night or on-demand.⁴¹

301 While this two-step process offers easier product separation compared to direct thermolysis, the
302 final products still need to be separated from unreacted H₂O or CO₂ and from the purge gas used to
303 dilute oxygen in the reduction step. Additionally, heating immense amounts of sweep gas (e.g. N₂)
304 incurs an energy penalty.⁵⁷ Alternative methods, including vacuum pumping and chemical
305 scavenging, have been investigated to reduce the partial pressure of oxygen and increase the
306 efficiency.^{58,59} The use of concentrated solar heat is a green alternative for upgrading the calorific
307 value of the fuel by adding solar energy in an amount equal to the enthalpy of the reaction.⁵⁵ Two-
308 step solar thermochemical cycles (**Figure 5b**) under concentrated irradiation using MO_{ox}/MO_{red}
309 (M=Zn, Ce, Fe) were reported to have a maximum η_{chem} of 20–40% for H₂ or CO production, though
310 this was dramatically affected by the operating conditions including heat recovery effectiveness,
311 temperatures, pressures, and solar irradiation concentration.^{60,61}

312 Such technologies provide an opportunity to use the waste heat in thermochemical processes. A
313 spectral splitting concentrator, consisting of upper and lower mirrors, has been proposed and designed
314 to achieve cascading utilisation of the full solar spectrum.⁶² The upper mirror allows the visible light
315 to be concentrated on photovoltaics, whereas the lower mirror enables the IR fraction to be focused
316 on a solar thermochemical reactor. Accordingly, a higher solar conversion efficiency (η) has been
317 estimated for such a hybrid system (19.0%) when compared to individual CPV (CdTe) (13.1%) and
318 thermochemical methanol decomposition systems (13.5%). Recently, thermodynamic evaluation of
319 a proposed concentrated photochemical-PV-thermochemical system that utilises the full solar

320 spectrum estimated a η of ~67%, with output products of photo-isomers, electricity, and syngas (H_2
321 + CO).⁶³ The thermalisation loss was diminished by recycling photons with $E > E_g$ for a
322 photochemical process (molecular isomerisation reaction) and employing the sub-bandgap photons
323 to provide heat for thermochemical methanol decomposition to produce syngas.

324 Solar thermophotovoltaics (STPV) provide another strategy with the potential to exceed the
325 Shockley–Queisser limit for PV by heating an intermediate absorber composed of a refractory metal
326 (e.g. W) with concentrated solar radiation and emitting narrowband radiation to PV cells.^{64,65} The
327 essential advantage of such a system is the ability to choose an emitter material with a selective
328 emission spectrum for illuminating the solar cell only with photons of $E = E_g$. Additionally, any
329 photons not absorbed by the PV will be reflected back to the emitter. Thus, in theory, the
330 thermalisation losses in a STPV system can be largely avoided, predicting a similar limiting η_{elec}
331 (85%) to an infinite tandem PV under 46200 suns (**Table 1**) when the intermediate absorber/emitter
332 is operated at 2544 K.⁶⁶ Although STPV-driven water electrolysis was expected to attain a η_{H_2} of
333 27% when efficiency of the thermal convertor was 80%,⁶⁷ experimental η of STPV remains modest
334 (< 30%),⁶⁸ mainly due to insufficient temperature control and inefficient energy transmission.^{43,65}

335

336 **Thermal and related approaches**

337 Even under 1 sun irradiation, photo(electro)chemical systems are generally heated by absorbed
338 sunlight via thermalisation, thermal heating, and radiative heat transfer by non-converted photons,
339 leading to an increased working temperature of 60–80 °C.⁶⁹ While excessive heating will reduce the
340 device lifetime and absorber efficiency,⁷⁰ careful manipulation of thermal energy to drive
341 complementary approaches may improve overall solar energy conversion efficiency. Solar thermal
342 technologies can take full advantage of solar IR radiation and are able to complement
343 photo(electro)chemical processes, as depicted in **Figure 5c, d, e**.

344

345 **Thermally accelerated photocatalysis.** High temperature is normally avoided in photovoltaic
346 applications due to its detrimental effect on the open-circuit voltage, particularly for CPV devices
347 where a cooling system is necessary to maintain optimal PV performance and minimise degradation.⁴⁴
348 However, the efficiency loss caused by increased temperatures is much smaller in
349 photoelectrochemical and photocatalytic systems due to cooling by the electrolyte solution and can
350 also be offset by improved reaction kinetics and electrolyte ion mobility, especially in a convective
351 flow system.⁷⁰

352 Recently, an integrated photoelectrochemical device for hydrogen generation via water splitting
353 over buried III–V-based photovoltaic components reached a η_{H_2} of 17.1% under an irradiance of up
354 to 474 suns owing to thermal integration, mass transport optimisation, and close electronic integration
355 between the photo-absorber and electrocatalyst.⁷¹ These results highlight that, compared to solar cell
356 devices where waste heat is highly undesirable, photoelectrochemical systems can take advantage of
357 thermal energy to enhance their performance. Such improvements are highly temperature dependent,
358 therefore necessitating careful device design to optimise the volume, flow rate, and depth of the
359 electrolyte layer above the photoelectrochemical devices for maximal efficiency.^{48,70}

360 The thermal effects in the IR region increase photocatalytic activity owing to enhanced reaction
361 kinetics on the semiconductor.⁷² According to the Arrhenius law, it can be estimated that catalytic
362 rates roughly double for every 10 °C increase in temperature.⁷³ Such thermal effects have been most
363 successfully exploited using a photocatalyst sheet consisting of Cr₂O₃/Ru-loaded SrTiO₃:La,Rh and
364 BiVO₄:Mo powder embedded into a gold layer, with record η_{H_2} of 1.1% for a pure water-splitting
365 reaction measured under 1 sun irradiation at elevated temperature (318 K), compared to ~0.3% at
366 room temperature.⁵

367 Another theoretical strategy for improving η_{chem} by utilising solar heating is through solar
368 thermal electrochemical photo (STEP) processes. The mechanistic basis of this technique is
369 decreasing the energy requirement for a chemical reaction, such as water or CO₂ splitting, by tuning
370 the electrochemical potential and kinetics with temperature.⁷⁴ For example, the electrolysis voltage
371 for water decreases with temperature from 1.229 V at 25 °C to 0.809 V at 600 °C and a H₂O partial
372 pressure of 500 bar.⁷⁵ The increased efficiency is derived from $\eta_{chem} = \eta_{elec} \times \eta_{electrolysis} \times A_{STEP}$
373 where A_{STEP} is the ratio of electrolysis voltage at ambient temperature over high temperature, and is
374 realised when the reactor is fully heated by solar IR that would otherwise go unused.⁷⁶ Although the
375 electrochemical basis for STEP processes has been experimentally validated by electrolysis of water
376 and CO₂ in molten salt solutions at 500 – 750 °C using low-potential electrolysis systems,^{77,78} true
377 experimental verification using solar heating and direct calculation of η_{chem} remains elusive. The
378 theoretical solar conversion efficiency limit for water and CO₂ splitting has been reported as >50%
379 and 54.7%, respectively.^{74,76}

380

381 **Pyroelectric and thermoelectric effect.** Thermal fluctuations and/or transient waste heat in the
382 operating environment have the potential to be harnessed by pyroelectric and thermoelectric materials
383 to provide voltage to support photo(electro)chemical reactions (**Figure 1e**).⁷⁹ Pyroelectric materials
384 rely on time-dependent temperature fluctuations that induce changes in polarisation of the material to
385 provide voltage.⁸⁰ An estimation has shown that electricity can be generated on pyroelectric materials
386 (Pb(Mg_{1/3}Nb_{2/3})O₃-PbTiO₃ single crystal) by natural temperature variations over 24 hours.⁸¹ The
387 coupling of pyroelectric effects with electrochemistry can be realised in either external or internal
388 configurations.⁸⁰ In an externally positioned system, the pyroelectric materials are not in direct contact
389 with the electrolyte and are instead simply used as a thermal energy harvester and source of charges
390 to drive electrochemical reactions. An internal system, where finely dispersed pyroelectric

391 particulates, for example $\text{Ba}_{0.7}\text{Sr}_{0.3}\text{TiO}_3$,⁸² are suspended in the reactant (*e.g.*, H_2O), can provide a
392 large pyroelectric surface area and total charge to stimulate H_2 production from water using thermal
393 fluctuations.

394 In contrast to pyroelectric materials that provide voltage from temperature fluctuations,
395 thermoelectric materials, such as Bi_2Te_3 , PbTe , Bi-Sb , and Si-Ge alloys,⁸³ rely on a temperature
396 gradient to transport charges based on the Seebeck effect. For example, a dark Ni nanosheet capable
397 of reaching an average temperature of $92\text{ }^\circ\text{C}$ within 2 min under simulated sunlight irradiation was
398 directly integrated on the hot end of thermoelectric generator for H_2 evolution from water.⁸⁴ The Ni
399 nanosheet not only provides sufficient temperature differences for thermoelectric generation but also
400 functions as a H_2 evolution catalyst, thereby improving water splitting overall.

401 Combining a photoelectrochemical module and a solar thermoelectric generator (**Figure 5e**)
402 would enable the utilisation of transmitted photons and waste heat, which can be directed to the
403 thermoelectric modules to generate electricity, leading to an increased η_{chem} . A conceptual design of
404 a thermoelectric-photoelectrochemical hybrid system was proposed to harness solar radiation and
405 waste heat, leading to efficient water splitting with $\eta_{\text{H}_2} \sim 20\%$ over a $56\text{ }^\circ\text{C}$ temperature gradient using
406 a Si photocathode wired to a Pt anode under 1 sun irradiation without an external applied voltage.⁸⁵
407 Integrating thermoelectric module in a tandem photoelectrochemical device also provides another
408 means of adjusting the J-V curve intersection point for the two individual photoelectrodes. Very recently,
409 a thermoelectric generator was directly mounted on the bottom of a photoelectrochemical cell
410 consisting of a Si photocathode and a BiVO_4 photoanode.⁸⁶ An additional bias of 100 mV was
411 generated from thermoelectric device by making use of the temperature difference between the
412 aqueous electrolyte warmed by incident sunlight irradiation and cooler, unirradiated water. The
413 addition of the thermoelectric system in this particular combination improved the

414 photoelectrochemical water splitting by a factor of 1.6 under 1 sun because the current J_{op} was
415 increased by shifting V_{op} , as shown in **Figure 4c**.

416 Although the full solar spectrum can be exploited by combining thermoelectric modules and
417 solar fuel production devices in the examples above, the efficiency enhancement of the hybrid system
418 is still modest. This is mainly due to the limitations of present integrated designs, which cannot
419 provide sufficient temperature gradients on the thermoelectric modules to deliver meaningful voltage.
420 According to the exergy and energy analysis, the maximal η_{elec} of solar-driven thermoelectric
421 generator under 1 sun irradiation was expected to be only $\sim 5\%$ (**Table 1**),⁸⁷ and current thermoelectric
422 technology is not yet cost-effective.⁸⁸ Future efforts should not only focus on the development of
423 high-efficiency, low-cost thermoelectric modules, but also the utilisation of concentrated solar light
424 to enhance the thermal effect and optimisation of the integrated design to maximise temperature
425 gradients and heat transfer.^{89,90} A simulation has estimated that the η_{elec} enhancement for integrating
426 thermoelectric device into a PV system is limited to 1.6% and 4.1% for p-type Si and copper indium
427 gallium selenide solar cell, respectively, due to large exergy losses.⁹¹ However, this exergy loss may
428 be reduced by using a PV cell with higher efficiency, thereby increasing the η_{chem} of thermoelectric
429 and PV-electrolysis hybrid systems.

430 The efficiency and output power of pyroelectric energy harvesting are expected to be greater
431 than thermoelectric methods due to their easier overall optimisation.⁸¹ The high thermal
432 conductivities typical of thermoelectric materials decrease the actual temperature gradient, making
433 practical implementation difficult. On the other hand, pyroelectric effects are limited by heat capacity,
434 a factor for which volumetric optimisation may easily compensate.

435

436 **Conclusions and Outlook**

437 A key challenge limiting the application of photo(electro)catalysis for artificial photosynthesis

438 is inefficient utilisation of the solar spectrum, resulting in more than half of the energy being lost as
439 waste heat. While there are still substantial efficiency benefits to be gained from improving and
440 understanding (photo)catalyst materials at a fundamental level, this review highlights how existing
441 complementary technologies can be coupled with photo(electro)chemical systems to increase solar
442 conversion efficiency and production rates. Adoption of solar fuel technologies can be accelerated
443 through exploring such complementary approaches which will improve the efficiency and economic
444 feasibility of such fuel production.

445 Of the techniques reviewed here, the most readily and widely applicable to most systems is that
446 of light management and solar spectrum adaptation. Instead of constraining photocatalyst absorbance
447 to match the solar spectrum, efficient photocatalysts may be selected for performance under ideal
448 illumination conditions and the solar spectrum may be adapted to meet these specifications. In
449 particular, hybrid up-/down-conversion systems capable of transforming a wide spectrum into a
450 tailored band of wavelengths have been shown to substantially improve η_{chem} . These up-/down-
451 conversion systems have benefited from considerable research efforts in recent years, making it
452 possible to immediately deploy this technology in existing solar fuel devices. For example, a filter
453 containing up-/down-conversion systems may be installed in front of the photocatalyst or light
454 absorber, or in some cases, up-/down-conversion materials might be deposited directly on, or be
455 suspended in a slurry with, the photocatalyst or light absorber.

456 Solar concentrators are components that can be relatively easily added to most solar fuels
457 systems to improve incident intensity, and they are anticipated to play an important part in the future
458 development of solar fuel technologies. In particular, PV-electrolysis and photoelectrochemical cells
459 would benefit from increased solar fuel production rate under concentrated light, leading to a reduced
460 embodied energy payback time, improving the sustainability and economic viability of such devices,
461 and allowing the use of more costly catalyst or PV components. Solar concentration can also be used

462 to gather heat which, with proper temperature management, may be used to improve reaction kinetics
463 or drive thermally activated processes.

464 While light management and solar concentration address the key issues of inefficient light
465 utilisation and increased production rate, integrated thermal approaches present a transformational
466 approach to solar fuels system design, presenting an opportunity to maximise solar energy conversion.
467 For example, thermally accelerated photocatalysis can be achieved by capturing solar heat to maintain
468 an optimal reaction temperature, further increasing the overall η_{chem} due to improved reaction
469 kinetics. IR radiation not typically absorbed by photocatalysts could instead be captured by thermal,
470 thermoelectric, and pyroelectric devices to generate extra bias or perform thermochemical processes,
471 complementing the light-driven devices. Such thermal approaches may also offer integrated solutions
472 to challenges such as the intermittent nature of solar energy. Heat collected during daytime operation
473 may reduce thermocatalysts which can then continue to drive fuel conversion processes at night.
474 While the potential benefits of such systems are great, the cost of integrating thermal approaches
475 should be justified by overall the efficiency gain of the system.

476 As an example of a device that approaches maximal utilisation of solar energy, we propose a
477 design that combines photo(electro)chemical processes, solar concentration, thermoelectric power
478 generation, and a thermal management strategy (**Figure 6a**). The integration of these various
479 technologies would lead to more efficient solar fuel production than the sum of each system applied
480 individually. A parabolic solar concentrator provides high solar irradiation intensity and abundant
481 heat to the integrated photoelectrochemical-thermoelectric generator, the thermoelectric element
482 utilises the heat gradient within the device to provide extra electrical bias, and the heat management
483 scheme is implemented to maintain the optimum device operating temperature while reusing the
484 excess heat to provide hot water for households and industry.

485 Although the integration of complementary technologies may improve the economic viability of
486 solar fuels processes, consideration of engineering design requirements to optimise implementation
487 of this technology is still important. The economic barrier-to-entry for artificial photosynthesis is
488 raised by the requirement for clean H₂O and CO₂ streams. By considering the design requirements
489 and available energy within the solar spectrum, engineering designs can implement strategic plant
490 locations and complementary approaches to maximise energy efficiency. Light management
491 strategies may direct IR irradiation not used by the photocatalytic process to drive desalination of
492 seawater and purification of wastewater using solar vapour generators (**Figure 1f**). Locating such a
493 solar fuel plant near the ocean and in close proximity to industrial sources of CO₂ will also reduce the
494 energy and financial cost required for reagent transportation which would be otherwise significant
495 considering the need for ~9,000 kg of water for every tonne of H₂ produced via water splitting (**Figure**
496 **6b**).⁹² Plant location should also be dictated by access to abundant sunlight, ideally at equator latitudes,
497 to maximise operating hours and shorten the energy and investment payback periods. Additionally,
498 although the produced gaseous mixture of hydrogen and oxygen from water splitting may be
499 separated by introducing molecular sieve membranes,⁹³ safely separating, transporting and storing
500 the produced H₂ still needs to be carefully considered as H₂ has a broad flammability range (4–94%
501 in O₂ at ambient temperature and pressure). Employing commercial electrolyzers (*e.g.*, polymer
502 electrolyte membrane electrolyzers) in PV-electrolysis can eliminate the need for product purification
503 and separation which can be challenging and costly.⁹⁴

504 The intermittent nature of solar energy remains a challenge to its utilisation. In order to minimise
505 the risk factor and provide uninterrupted and reliable fuel production, round-the-clock fuel production
506 photocatalysts and systems are desirable.⁹⁵ For example, an integrated photoelectrochemical-
507 electrolysis system that performs photoelectrochemical reactions under sunlight irradiation and
508 utilises renewable electricity, such as generated by wind or hydropower, to drive electrolysis at night

509 has also been proposed recently.⁹⁶

510 Industrialisation of solar fuels is a critical and revolutionary step toward a sustainable energy
511 system. While the materials and device architecture for artificial photosynthetic systems can still be
512 improved in terms of light utilisation and energy conversion efficiency, such improvements are also
513 possible through considered engineering design to integrate complementary technologies. Global
514 adoption of solar-powered sustainable processes is dependent on multidisciplinary collaboration
515 between scientists, engineers, and industry to establish the feasibility and design of such systems.

516

517 **Acknowledgements**

518 We thank Dr Christian Pichler of the University of Cambridge and Dr Wolfgang Hofer from OMV
519 for helpful discussions. This work was supported by an EU Marie Skłodowska-Curie Individual
520 Fellowships (GAN 793996 to Q.W.), the JSPS Leading Initiative for Excellent Young Researchers
521 (to Q.W.), the Cambridge Trust (Cambridge Thai Foundation Award to C.P.), a Trinity-Henry Barlow
522 Scholarship (to C.P.), an NSERC Postdoctoral Fellowship (to S.L.), and the OMV Group (to E.R.).

523

524 **Competing interests**

525 The authors declare no competing interests.

526

527 **Table 1 | Theoretical limits of solar energy conversion efficiency.** The limiting efficiencies for
 528 these solar-driven processes are based on thermodynamic considerations, assuming no losses during
 529 the current-chemical conversion ($\eta_{chem} = \eta_{elec}$).

		η (1 sun) (%)	η (concentrated) (%)
PV-electrolysis	Single light absorber ^a	~67	~86
Photoelectrochemistry	(without thermalisation losses)		
Photocatalysis	Single light absorber ^b	~30	~40
	(with thermalisation losses)		
	Dual light absorbers ^c	~42	~ ^k
	(with thermalisation losses)		
	Infinite tandem ^d	~67	~86
	Single light absorber	~43	~ ^k
	(with up-conversion) ^e		
	Single light absorber	~40	~ ^k
	(with down-conversion) ^f		
	Single light absorber	~45	~ ^k
	(with combined up- and down-conversion) ^g		
Two-step solar thermochemical cycles ^h		~ ^j	~20–40
Thermoelectric generator ⁱ		~5	~ ^k

530 ^a Assumptions: (1) Only radiative recombination takes place (no leak and accumulation of electrons and holes); (2) No
 531 thermalisation losses; (3) Rate of generation is at maximum; (4) No losses due to electrode polarisation and overpotential;
 532 (5) Device operating temperature is 300 K (concentrated sunlight: 45900 suns). Data were obtained from refs. 6, 11.

533 ^b No losses due to electrode polarisation and overvoltage. Device operating temperature is 300 K (concentrated sunlight:
 534 45900). Data were obtained from refs. 11.

535 ^c No losses due to electrode polarisation and overvoltage. Device operating temperature is 300 K (concentrated sunlight:
 536 45900 suns). The bandgaps of the light absorbers are 1.0 and 1.9 eV, respectively. Data were obtained from ref. 11.

537 ^d No losses due to electrode polarisation and overvoltage. Device operating temperature is 300 K (concentrated sunlight:
 538 45900 suns). Data were obtained from refs. 6, 11.

539 ^e Bandgap is 1.76 eV. Device operating temperature is 300 K. Data were obtained from refs. 28.

540 ^f Bandgap is ~1.0 eV. Device operating temperature is 300 K. Data were obtained from refs. 28, 29.

541 ^g Bandgap is 0.9–1.4 eV. Device operating temperature is 300 K. Data were obtained from ref. 28.

542 ^h Two-step solar thermochemical cycles with MO_{red}/MO_{ox} (M=Zn, Ce, Fe). For $CO_2 \rightarrow CO + \frac{1}{2}O_2$ and water splitting
 543 using CeO/CeO_{2- δ} , the reduction and oxidation temperatures are 1805.4 and 1000 K, respectively. For $CO_2 \rightarrow CO + \frac{1}{2}O_2$
 544 using Zn/ZnO and FeO/Fe₃O₄, the reduction and oxidation temperatures are 2000 and 298 K, respectively. Data were
 545 obtained from refs. 60, 61.

546 ⁱ Data were obtained from refs. 87, 97. The cold and hot side temperatures are ~293 and ~470 K, respectively.

547 ^j “~” indicates “Not applicable”.

548 ^k “~” indicates “Lack of available data”.

549

550 **Figure 1 | Solar energy conversion technologies.** a-c, Schematic representation of particulate
 551 photocatalysis (a), photoelectrochemistry (b), and photovoltaic-powered electrolysis (c) for solar-to-
 552 chemical conversion. d-f, Schematic illustrations of complementary conversion technologies that can
 553 take advantage of the IR component of the solar spectrum, including solar-powered thermocatalysis

554 (d), a solar-driven thermoelectric/pyroelectric generator (e) and a solar vapour generator (f). UV, Vis,
555 IR represent ultraviolet, visible, and infrared light, respectively.

556

557 **Figure 2 | Solar-to-hydrogen conversion efficiencies (η_{H_2}) for selected water splitting systems.**

558 The triangles, squares, and circles indicate particulate photocatalytic systems (PC), bias-free
559 photoelectrochemical cells (PEC), and photovoltaic-powered electrochemical cells (PV-electrolysis),
560 respectively under 1 sun irradiation. The absorption edge of the device was determined by the light
561 receiver with smaller bandgap. The AM1.5G solar spectrum is based on the ASTM G173-03 reference
562 spectrum, and the cumulative energy content as a function wavelength are shown in the grey and blue
563 curves, respectively, for comparison. Data were obtained from ref. 4 (SrTiO₃:Al), ref. 5 (BiVO₄:Mo-
564 SrTiO₃:La,Rh sheet), ref. 14 (BiVO₄:Mo-CIGS), ref. 13 (BiVO₄:Mo-Cu₂O), ref. 98 (Ta₃N₅-CuInSe₂),
565 ref. 15 (GaInP-GaInAs), ref. 99 (Perovskite-NiFe), and ref. 100 (*multi* Si-Ni).

566

567 **Figure 3 | Light management for hybrid systems. a,** The utilisation of a beam splitter to separate
568 incident sunlight and direct each band to the most efficient convertor. **b,** A photoelectrochemical
569 system using a photoanode with a light-trapping layer on its back to recycle short-wavelength photons.
570 The yellow, blue, and red arrows represent incident light, short-wavelength photons, and long-
571 wavelength photons, respectively. UV, Vis, NIR, IR represent ultraviolet, visible, near-infrared and
572 infrared light, respectively.

573

574 **Figure 4 | Photon wavelength manipulation using up- and down-conversion for**
575 **photo(electro)chemical systems. a-b,** Schematic illustrations of photocatalysts combined with a
576 downconverter (**a**) and downshifter (**b**). **c,** Illustration showing the expected effect of light adaptation
577 on the performance of a bias-free photoelectrochemical system. J_{op} : operating current density. V_{op} :

578 operating potential. The current density–voltage (J-V) curves of photoanode and photocathode are
579 represented in pink and blue, respectively. The dotted, dashed and solid curves represent ideal J-V
580 behaviour, real J-V performance and predicted J-V performance with light adaption, respectively. **d-**
581 **e**, Schematic illustrations of upconversion mechanisms for photocatalysts combined with Ln-doped
582 upconverter (**d**) and triplet-triplet annihilation upconverter (**e**). E_1 , E_2 , and E_3 are excited states, and
583 S_1 , and T_1 are excited singlet states and triplet states, respectively. Ln represents lanthanide. UV,
584 NIR represent ultraviolet and near-infrared light, respectively.

585

586 **Figure 5 | Solar concentrator and thermal related approaches.** **a**, Schematic illustration of a
587 tracking-integrated concentrating system for a photoelectrochemical device. **b-e**, Illustration showing
588 solar-powered two-step thermochemical fuel synthesis (**b**), thermally accelerated photocatalysis (**c**),
589 thermally-assisted photoelectrochemical fuel synthesis (**d**) and solar fuel synthesis using
590 thermoelectric-assisted photoelectrochemical processes (**e**). NIR represents near-infrared light.

591

592 **Figure 6 | Systems combining solar thermal approaches and photo(electro)chemical processes.**
593 **a**, An integrated system consisting of a photoelectrochemical cell, a solar concentrator and a
594 thermoelectric generator with thermal management. **b**, The utilisation of water vapour and waste CO_2
595 feedstocks provided by a solar vapour generator and a factory, respectively, for artificial
596 photosynthetic systems.

597

598 **References**

599 1. Kim, J. H., Hansora, D., Sharma, P., Jang, J.-W. & Lee, J. S. Toward practical solar hydrogen
600 production – an artificial photosynthetic leaf-to-farm challenge. *Chem. Soc. Rev.* **48**, 1908–1971
601 (2019).

- 602 2. Shaner, M. R., Atwater, H. A., Lewis, N. S. & McFarland, E. W. A comparative technoeconomic
603 analysis of renewable hydrogen production using solar energy. *Energy Environ. Sci.* **9**, 2354–
604 2371 (2016).
- 605 3. McKone, J. R., Lewis, N. S. & Gray, H. B. Will solar-driven water-splitting devices see the light
606 of day? *Chem. Mater.* **26**, 407–414 (2014).
- 607 4. Takata, T. *et al.* Photocatalytic water splitting with a quantum efficiency of almost unity. *Nature*
608 **581**, 411–414 (2020).
- 609 5. Wang, Q. *et al.* Scalable water splitting on particulate photocatalyst sheets with a solar-to-
610 hydrogen energy conversion efficiency exceeding 1%. *Nat. Mater.* **15**, 611–615 (2016).
- 611 6. Würfel, P. Thermodynamic limitations to solar energy conversion. *Physica E: Low-dimens. Syst.*
612 *Nanostruct.* **14**, 18–26 (2002).
- 613 **Study reporting the thermodynamic analysis and entropy-limited ideal maximum**
614 **efficiency of solar energy conversion process.**
- 615 7. Huang, X., Han, S., Huang, W. & Liu, X. Enhancing solar cell efficiency: The search for
616 luminescent materials as spectral converters. *Chem. Soc. Rev.* **42**, 173–201 (2013).
- 617 8. Shockley, W. & Queisser, H. J. Detailed balance limit of efficiency of p-n junction solar cells.
618 *J. Appl. Phys.* **32**, 510–519 (1961).
- 619 9. Wang, Q. & Domen, K. Particulate photocatalysts for light-driven water splitting: Mechanisms,
620 challenges, and design strategies. *Chem. Rev.* **120**, 919–985 (2019).
- 621 10. Wang, Y. *et al.* Mimicking natural photosynthesis: Solar to renewable H₂ fuel synthesis by Z-
622 scheme water splitting systems. *Chem. Rev.* **118**, 5201–5241 (2018).
- 623 11. De Vos, A. Detailed balance limit of the efficiency of tandem solar cells. *J. Phys. D: Appl. Phys.*
624 **13**, 839–846 (1980).

- 625 12. Hu, S., Xiang, C., Haussener, S., Berger, A. D. & Lewis, N. S. An analysis of the optimal band
626 gaps of light absorbers in integrated tandem photoelectrochemical water-splitting systems.
627 *Energy Environ. Sci* **6**, 2984–2993 (2013).
- 628 13. Pan, L. *et al.* Boosting the performance of Cu₂O photocathodes for unassisted solar water
629 splitting devices. *Nat. Catal.* **1**, 412–420 (2018).
- 630 14. Kobayashi, H. *et al.* Development of highly efficient CuIn_{0.5}Ga_{0.5}Se₂-based photocathode and
631 application to overall solar driven water splitting. *Energy Environ. Sci.* **11**, 3003–3009 (2018).
- 632 15. Cheng, W.-H. *et al.* Monolithic photoelectrochemical device for direct water splitting with 19%
633 efficiency. *ACS Energy Lett.* **3**, 1795–1800 (2018).
- 634 16. Bolton, J. R., Strickler, S. J. & Connolly, J. S. Limiting and realizable efficiencies of solar
635 photolysis of water. *Nature* **316**, 495–500 (1985).
- 636 17. Mojiri, A., Taylor, R., Thomsen, E. & Rosengarten, G. Spectral beam splitting for efficient
637 conversion of solar energy—A review. *Renew. Sust. Energy Rev.* **28**, 654–663 (2013).
- 638 18. Acar, C. & Dincer, I. Enhanced generation of hydrogen, power, and heat with a novel integrated
639 photoelectrochemical system. *Int. J. Hydrogen Energy*, **45**, 34666–34667 (2020).
- 640 19. Qiu, Y. *et al.* Efficient solar-driven water splitting by nanocone BiVO₄-perovskite tandem cells.
641 *Sci. Adv.* **2**, e1501764 (2016).
- 642 20. Skoplaki, E. & Palyvos, J. A. On the temperature dependence of photovoltaic module electrical
643 performance: A review of efficiency/power correlations. *Sol. Energy* **83**, 614–624 (2009).
- 644 21. Imenes, A. G., Buie, D. & McKenzie, D. The design of broadband, wide-angle interference
645 filters for solar concentrating systems. *Sol. Energy Mater. Sol. Cells* **90**, 1579–1606 (2006).
- 646 22. Na, S.-I. *et al.* Efficient polymer solar cells with surface relief gratings fabricated by simple soft
647 lithography. *Adv. Funct. Mater.* **18**, 3956–3963 (2008).

- 648 23. Zeng, L. *et al.* Demonstration of enhanced absorption in thin film Si solar cells with textured
649 photonic crystal back reflector. *Appl. Phys. Lett.* **93**, 221105 (2008).
- 650 24. Mokkalapati, S. & Catchpole, K. R. Nanophotonic light trapping in solar cells. *J. Appl. Phys.* **112**,
651 101101 (2012).
- 652 25. Shi, X. *et al.* Unassisted photoelectrochemical water splitting exceeding 7% solar-to-hydrogen
653 conversion efficiency using photon recycling. *Nat. Commun.* **7**, 11943 (2016).
- 654 **Light management enhanced photocurrent generation for photoelectrochemical water**
655 **splitting using a distributed Bragg reflector.**
- 656 26. Rao, A. & Friend, R. H. Harnessing singlet exciton fission to break the Shockley–Queisser limit.
657 *Nat. Rev. Mater.* **2**, 17063 (2017).
- 658 27. Smith, M. B. & Michl, J. Singlet Fission. *Chem. Rev.* **110**, 6891–6936 (2010).
- 659 28. Tayebjee, M. J., Rao, A. & Schmidt, T. All-optical augmentation of solar cells using a
660 combination of up- and downconversion. *J. Photonics Energy*, **8**, 022007 (2018).
- 661 **A detailed study on the effects of up- and down-conversion on the theoretical maximum**
662 **efficiency of solar cells.**
- 663 29. Tayebjee, M. J. Y., Gray-Weale, A. A. & Schmidt, T. W. Thermodynamic limit of exciton fission
664 solar cell efficiency. *J. Phys. Chem. Lett.* **3**, 2749–2754 (2012).
- 665 30. Hovel, H. J., Hodgson, R. T. & Woodall, J. M. The effect of fluorescent wavelength shifting on
666 solar cell spectral response. *Sol. Energy Mater.* **2**, 19–29 (1979).
- 667 31. Wen, S. *et al.* Future and challenges for hybrid upconversion nanosystems. *Nat. Photonics* **13**,
668 828–838 (2019).
- 669 32. Rahaman, M. *et al.* Selective CO production from aqueous CO₂ using a Cu₉In₄ catalyst and its
670 integration into a bias-free solar perovskite–BiVO₄ tandem device. *Energy Environ. Sci.* **13**,
671 3536–3543 (2020).

- 672 33. Choi, D., Nam, S. K., Kim, K. & Moon, J. H. Enhanced photoelectrochemical water splitting
673 through bismuth vanadate with a photon upconversion luminescent reflector. *Angew. Chem. Int.*
674 *Ed.* **131**, 6965–6969 (2019).
- 675 **A demonstration of combined up- and down-conversion to increase the efficiency of**
676 **photoelectrochemical water splitting.**
- 677 34. Trupke, T., Green, M. & Würfel, P. Improving solar cell efficiencies by up-conversion of sub-
678 band-gap light. *J. Appl. Phys.* **92**, 4117–4122 (2002).
- 679 35. Zhang, M. *et al.* Improving hematite’s solar water splitting efficiency by incorporating rare-earth
680 upconversion nanomaterials. *J. Phys. Chem. Lett.* **3**, 3188–3192 (2012).
- 681 36. Wang, X. *et al.* Dye-sensitized lanthanide-doped upconversion nanoparticles. *Chem. Soc. Rev.*
682 **46**, 4150–4167 (2017).
- 683 37. Singh-Rachford, T. N. & Castellano, F. N. Photon upconversion based on sensitized triplet-
684 triplet annihilation. *Coord. Chem. Rev.* **254**, 2560–2573 (2010).
- 685 38. Gholizadeh, E. M. *et al.* Photochemical upconversion of near-infrared light from below the
686 silicon bandgap. *Nat. Photonics* **14**, 585–590 (2020).
- 687 39. Kim, J.-H. & Kim, J.-H. Encapsulated triplet-triplet annihilation-based upconversion in the
688 aqueous phase for sub-band-gap semiconductor photocatalysis. *J. Am. Chem. Soc.* **134**, 17478–
689 17481 (2012).
- 690 40. Kroupa, D. M., Roh, J. Y., Milstein, T. J., Creutz, S. E. & Gamelin, D. R. Quantum-cutting
691 ytterbium-doped CsPb(Cl_{1-x}Br_x)₃ perovskite thin films with photoluminescence quantum yields
692 over 190%. *ACS Energy Lett.* **3**, 2390–2395 (2018).
- 693 41. Romero, M. & Steinfeld, A. Concentrating solar thermal power and thermochemical fuels.
694 *Energy Environ. Sci.* **5**, 9234–9245 (2012).

- 695 42. Lewis M. Fraas, L. D. P. *Solar Cells and Their Applications, 2nd Edition*. (John Wiley & Sons,
696 Inc., 2010).
- 697 43. Green, M. A. & Bremner, S. P. Energy conversion approaches and materials for high-efficiency
698 photovoltaics. *Nat. Mater.* **16**, 23–34 (2017).
- 699 44. Jia, J. *et al.* Solar water splitting by photovoltaic-electrolysis with a solar-to-hydrogen efficiency
700 over 30%. *Nat. Commun.*, **7**, 1–6 (2016).
- 701 **A record demonstration of η_{H_2} efficiency achieved by solar PV-electrolysis under 42 suns**
702 **concentrated irradiation.**
- 703 45. Geisz, J. F. *et al.* Six-junction III–V solar cells with 47.1% conversion efficiency under 143 Suns
704 concentration. *Nat. Energy* **5**, 326–335 (2020).
- 705 46. Rodriguez, C. A., Modestino, M. A., Psaltis, D. & Moser, C. Design and cost considerations for
706 practical solar-hydrogen generators. *Energy Environ. Sci.* **7**, 3828–3835 (2014).
- 707 47. Holmes-Gentle, I., Tembhurne, S., Suter, C. & Haussener, S. Dynamic system modeling of
708 thermally-integrated concentrated PV-electrolysis. *Int. J. Hydrog. Energy* **46**, 10666–10681
709 (2021).
- 710 48. Khan, M., Shankiti, I., Ziani, A., Wehbe, N. & Idriss, H. A stable integrated
711 photoelectrochemical reactor for H₂ production from water attains a solar-to-hydrogen
712 efficiency of 18% at 15 suns and 13% at 207 suns. *Angew.Chem. Int. Ed.* **59**, 14802–14808
713 (2020).
- 714 49. Uekert, T., Pichler, C. M., Schubert, T. & Reisner, E. Solar-driven reforming of solid waste for
715 a sustainable future. *Nat. Sustain.* **4**, 383–391 (2021).
- 716 50. Castedo, A., Casanovas, A., Angurell, I., Soler, L. & Llorca, J. Effect of temperature on the gas-
717 phase photocatalytic H₂ generation using microreactors under UVA and sunlight irradiation.
718 *Fuel* **222**, 327–333 (2018).

- 719 51. Castedo, A., Uriz, I., Soler, L., Gandía, L. M. & Llorca, J. Kinetic analysis and CFD simulations
720 of the photocatalytic production of hydrogen in silicone microreactors from water-ethanol
721 mixtures. *Appl. Catal., B* **203**, 210–217 (2017).
- 722 52. Wei, Q. et al. Direct solar photocatalytic hydrogen generation with CPC photoreactors: System
723 development. *Sol. Energy* **153**, 215–223 (2017).
- 724 **A demonstration of a scalable photocatalytic hydrogen production system under**
725 **concentrated solar irradiation from compound parabolic collectors.**
- 726 53. Apostoleris, H., Stefancich, M. & Chiesa, M. Tracking-integrated systems for concentrating
727 photovoltaics. *Nat. Energy* **1**, 16018 (2016).
- 728 54. Chueh, W. C. et al. High-flux solar-driven thermochemical dissociation of CO₂ and H₂O using
729 nonstoichiometric ceria. *Science* **330**, 1797–1801 (2010).
- 730 **A demonstration of two-step, solar-driven thermochemical production of fuels.**
- 731 55. Steinfeld, A. Solar thermochemical production of hydrogen—A review. *Sol. Energy* **78**, 603–
732 615 (2005).
- 733 56. Muhich, C. L. et al. Efficient generation of H₂ by splitting water with an isothermal redox cycle.
734 *Science* **341**, 540–542 (2013).
- 735 57. Lapp, J., Davidson, J. H. & Lipiński, W. Efficiency of two-step solar thermochemical non-
736 stoichiometric redox cycles with heat recovery. *Energy* **37**, 591–600 (2012).
- 737 58. Ermanoski, I., Siegel, N. P. & Stechel, E. B. A new reactor concept for efficient solar-
738 thermochemical fuel production. *J. Sol. Energy Eng.* **135**, 031002 (2013).
- 739 59. Lin, M. & Haussener, S. Solar fuel processing efficiency for ceria redox cycling using alternative
740 oxygen partial pressure reduction methods. *Energy* **88**, 667–679 (2015).

- 741 60. Gálvez, M. E., Loutzenhiser, P. G., Hischer, I. & Steinfeld, A. CO₂ splitting via two-step solar
742 thermochemical cycles with Zn/ZnO and FeO/Fe₃O₄ redox reactions: thermodynamic analysis.
743 *Energy Fuels* **22**, 3544–3550 (2008).
- 744 61. Scheffe, J. R. & Steinfeld, A. Thermodynamic analysis of cerium-based oxides for solar
745 thermochemical fuel production. *Energy Fuels* **26**, 1928–1936 (2012).
- 746 62. Qu, W., Hong, H. & Jin, H. A spectral splitting solar concentrator for cascading solar energy
747 utilization by integrating photovoltaics and solar thermal fuel. *Appl. Energy* **248**, 162–173
748 (2019).
- 749 63. Fang, J. *et al.* Thermodynamic evaluation of a concentrated photochemical–photovoltaic–
750 thermochemical (CP-PV-T) system in the full-spectrum solar energy utilization. *Appl. Energy*
751 **279**, 115778 (2020).
- 752 64. Kolm, H. H. Solar-battery power source. *Quarterly Progress Report Solid State Research* (MIT
753 Lincoln Laboratory, 1965).
- 754 65. Wang, Y., Liu, H. & Zhu, J. Solar thermophotovoltaics: Progress, challenges, and opportunities.
755 *APL Mater.* **7**, 080906 (2019).
- 756 66. Harder, N.-P. & Würfel, P. Theoretical limits of thermophotovoltaic solar energy conversion.
757 *Semicond. Sci. Technol.* **18**, S151–S157 (2003).
- 758 67. Rabaday, R. I. & Kanaan, B. Power spectral shaping for hydrogen production from silicon based
759 hybrid thermo-photovoltaic water electrolysis. *Energy* **133**, 1–8 (2017).
- 760 68. Omair, Z. *et al.* Ultraefficient thermophotovoltaic power conversion by band-edge spectral
761 filtering. *Proc. Natl. Acad. Sci. U. S. A.* **116**, 15356–15361 (2019).
- 762 69. Urbain, F. *et al.* Influence of the operating temperature on the performance of silicon based
763 photoelectrochemical devices for water splitting. *Mater. Sci. Semicond. Process.* **42**, 142–146
764 (2016).

- 765 70. Haussener, S., Hu, S., Xiang, C., Weber, A. Z. & Lewis, N. S. Simulations of the irradiation and
766 temperature dependence of the efficiency of tandem photoelectrochemical water-splitting
767 systems. *Energy Environ. Sci* **6**, 3605–3618 (2013).
- 768 71. Tembhrne, S., Nandjou, F. & Haussener, S. A thermally synergistic photo-electrochemical
769 hydrogen generator operating under concentrated solar irradiation. *Nat. Energy* **4**, 399–407
770 (2019).
- 771 **Study representing an efficient photoelectrochemical device under concentrated**
772 **irradiation with thermal integration and highlighting that photoelectrochemical systems**
773 **can take advantage of thermal energy to enhance their performance.**
- 774 72. Hisatomi, T., Minegishi, T. & Domen, K. Kinetic assessment and numerical modeling of
775 photocatalytic water splitting toward efficient solar hydrogen production. *Bull. Chem. Soc. Jpn.*
776 **85**, 647–655 (2012).
- 777 73. van de Krol, R. & Parkinson, B. A. Perspectives on the photoelectrochemical storage of solar
778 energy. *MRS Energy Sustain.* **4**, E13 (2017).
- 779 74. Licht, S. Efficient solar-driven synthesis, carbon capture, and desalinization, STEP: solar
780 thermal electrochemical production of fuels, metals, bleach. *Adv. Mater.* **23**, 5592–5612 (2011).
- 781 75. Licht, S. Solar water splitting to generate hydrogen fuel—a photothermal electrochemical
782 analysis. *Int. J. Hydrog. Energy* **30**, 459–470 (2005).
- 783 76. Licht, S. STEP (Solar thermal electrochemical photo) generation of energetic molecules: A solar
784 chemical process to end anthropogenic global warming. *J. Phys. Chem. C* **113**, 16283–16292
785 (2009).
- 786 77. Licht, S., Halperin, L., Kalina, M., Zidman, M. & Halperin, N. Electrochemical potential tuned
787 solar water splitting. *Chem. Commun.* **24**, 3006–3007 (2003).

- 788 78. Licht, S., Cui, B. & Wang, B. STEP carbon capture – The barium advantage. *J. CO₂ Util.* **2**, 58–
789 63 (2013).
- 790 79. Mulla, R. & Dunnill, C. W. Powering the hydrogen economy from waste heat: A review of heat-
791 to-hydrogen concepts. *ChemSusChem* **12**, 3882–3895 (2019).
- 792 80. Zhang, Y. *et al.* Thermal energy harvesting using pyroelectric-electrochemical coupling in
793 ferroelectric materials. *Joule* **4**, 301–309 (2020).
- 794 81. Sebald, G., Guyomar, D. & Agbossou, A. On thermoelectric and pyroelectric energy harvesting.
795 *Smart Mater. Struct.* **18**, 125006 (2009).
- 796 82. Xu, X. *et al.* Pyro-catalytic hydrogen evolution by Ba_{0.7}Sr_{0.3}TiO₃ nanoparticles: harvesting cold–
797 hot alternation energy near room-temperature. *Energy Environ. Sci.* **11**, 2198–2207 (2018).
- 798 83. Li, J.-F., Liu, W.-S., Zhao, L.-D. & Zhou, M. High-performance nanostructured thermoelectric
799 materials. *NPG Asia Mater.* **2**, 152–158 (2010).
- 800 84. Zhao, L. *et al.* An earth-abundant and multifunctional Ni nanosheets array as electrocatalysts
801 and heat absorption layer integrated thermoelectric device for overall water splitting. *Nano*
802 *Energy* **56**, 563–570 (2019).
- 803 85. Shin, S.-M., Jung, J.-Y., Park, M.-J., Song, J.-W. & Lee, J.-H. Catalyst-free hydrogen evolution
804 of Si photocathode by thermovoltage-driven solar water splitting. *J. Power Sources* **279**, 151–
805 156 (2015).
- 806 86. Kang, Y. *et al.* An integrated thermoelectric-assisted photoelectrochemical system to boost
807 water splitting. *Sci. Bull.* **65**, 1163–1169 (2020).
- 808 **Report integrating a thermoelectric generator in a photoelectrochemical system for full**
809 **solar spectrum utilisation and enhanced hydrogen production.**
- 810 87. Chen, J. Thermodynamic analysis of a solar-driven thermoelectric generator. *J. Appl. Phys.* **79**,
811 2717–2721(1996).

- 812 88. Yang, D. & Yin, H. Energy conversion efficiency of a novel hybrid solar system for photovoltaic,
813 thermoelectric, and heat utilization. *IEEE Trans. Energy Convers.* **26**, 662–670 (2011).
- 814 89. Tomeš, P., Suter, C., Trottmann, M., Steinfeld, A. & Weidenkaff, A. Thermoelectric oxide
815 modules tested in a solar cavity-receiver. *J. Mater. Res.* **26**, 1975–1982, (2011)
- 816 90. Kraemer, D. *et al.* Concentrating solar thermoelectric generators with a peak efficiency of 7.4%.
817 *Nat. Energy* **1**, 16153 (2016).
- 818 **Study highlighting that future efforts on the combination of thermoelectric modules and**
819 **solar fuel production should focus on the utilisation of concentrated solar light to enhance**
820 **the thermal effect.**
- 821 91. Li, D., Xuan, Y., Li, Q. & Hong, H. Exergy and energy analysis of photovoltaic-thermoelectric
822 hybrid systems. *Energy* **126**, 343–351 (2017).
- 823 92. Pinaud, B. A. *et al.* Technical and economic feasibility of centralized facilities for solar hydrogen
824 production via photocatalysis and photoelectrochemistry. *Energy Environ. Sci.* **6**, 1983–2002
825 (2013).
- 826 93. Leelachaikul, P. *et al.* Perfluorooctanol-based liquid membranes for H₂/O₂ separation. *Sep. Purif.*
827 *Technol.* **122**, 431–439 (2014).
- 828 94. Andersson, J. & Grönkvist, S. Large-scale storage of hydrogen. *Int. J. Hydrog. Energy* **44**,
829 11901–11919 (2019).
- 830 95. Lau, V. W.-h. *et al.* Dark photocatalysis: storage of solar energy in carbon nitride for time-
831 delayed hydrogen generation. *Angew. Chem. Int. Ed.* **56**, 510–514 (2017).
- 832 96. Pornrungroj, C. *et al.* Bifunctional perovskite-BiVO₄ tandem devices for uninterrupted solar and
833 electrocatalytic water splitting cycles. *Adv. Funct. Mater.* **31**, 2008182 (2021)
- 834 97. Bellos, E. & Tzivanidis, C. Energy and financial analysis of a solar driven thermoelectric
835 generator. *J. Clean. Prod.* **264**, 121534 (2020).

- 836 98. Higashi, T. *et al.* Transparent Ta₃N₅ photoanodes for efficient oxygen evolution toward the
837 development of tandem cells. *Angew. Chem. Int. Ed.* **58**, 2300–2304 (2019).
- 838 99. Luo, J. *et al.* Water photolysis at 12.3% efficiency via perovskite photovoltaics and Earth-
839 abundant catalysts. *Science* **345**, 1593–1596 (2014).
- 840 100. Schüttauf, J.-W. *et al.* Solar-to-hydrogen production at 14.2% efficiency with silicon
841 photovoltaics and earth-abundant electrocatalysts. *J. Electrochem. Soc.* **163**, F1177–F1181,
842 (2016).
- 843